Supporting Information

Unveiling the Triple Enhancement Mechanism of Phosphorus Doping: A Carbon Cathode with Precise Mesoporous Structure for Advanced Zinc-Ion Energy Storage

Yongtao Sun [a,b,1], Ying Li [a,1], Huihui Li [b], Shengqin Guan [b], Jianlong Wang [b], Binbin Zhang [b], Shengliang Hu [a,*], Kaixi Li [b,*], Taotao Guan [b,*]

[a] Research Group of New Energy Materials and Devices, State Key Laboratory of Coal and CBM Co-Mining, North University of China, Taiyuan 030051, PR China

[b] Shanxi Key Laboratory of Carbon Materials, Institute of Coal Chemistry, Chi nese Academy of Sciences, Taiyuan 030001, PR China

[*] Corresponding authors

E-mail addresses: hsliang@yeah.net(S. Hu), likx@sxicc.ac.cn(K. Li), guantt@hot mail.com(T. Guan).

Contents

1. Supporting Experimental Section

1.1 Electrode preparation and Zn-ion hybrid supercapacitors assembly (ZIHCs)

To fabricate the working electrode, a mixture was first prepared by dispersing porous carbon, conductive carbon black, and polyvinylidene fluoride (PVDF) binder in N-methylpyrrolidone (NMP)—with the three components mixed at an 8:1:1 weight ratio. This slurry was then evenly spread onto a stainless steel mesh; during this step, the loading of active material was controlled to fall within the range of 1.0-2.0 mg cm^{-2}. After coating, the mesh with the slurry was placed in a vacuum oven and dried at 80°C for 12 hours to complete the working electrode preparation. For electrochemical performance testing, CR2032 coin-type zinc-ion hybrid supercapacitors (ZIHCs) were assembled first, and their performance was assessed under room-temperature conditions. The assembled cells featured a specific configuration: a zinc foil served as the anode, a glass fiber membrane acted as the separator, a porous carbon-based material functioned as the cathode, and 2 mol L^{-1} $ZnSO_4$ solution was used as the electrolyte.

1.2 Electrochemical equations and calculations

Cyclic voltammetry (CV) and electrochemical impedance spectroscopy (EIS) were measured on a CHI 660E electrochemical workstation (Chenhua Instruments Co. China) at room temperature. A LAND CT3001A battery test system (Wuhan LAND Electronics Co., Ltd., China) was employed to obtain galvanostatic charge-discharge (GCD) curves, XPS measurements were carried out on a Thermo Fisher Scientific Nexsa G2 (USA) spectrometer using a monochromatic Al Kα X-ray source (*hv* =

1486.6 eV) operated at 120 W.

The defect density of the material is obtained based on Raman testing, and the formula is described as follows:

$$n_D = 1.8 \times 10^{22} \times (I_D \times I_G)/L^4 \#（S1）$$ λ

where λ_L = 532 nm.

The valence band position relative to the standard hydrogen electrode is obtained based on VB-XPS testing, and the formula is as follows:

$$E_{VB,NHE} = E_{VB-XPS} + \varphi - 4.4 \#（S2）$$

Among them, $E_{VB,NHE}$ is the potential of the valence band relative to the standard hydrogen electrode, $E_{VB\text{-}XPS}$ is the valence band value measured by VB-XPS, and φ is the instrument work function (taken as 4.2 eV) [1].

The charge storage dynamics and capacitance contribution are obtained based on CV results testing, and the formula is as follows:

$$i(v) = av^b \#（S3）$$

Or convert it into the following formula:

$$logi(v) = log(a) + blog\ (v) \#（S4）$$

Where i (A g^{-1}) represents the total current response, v (mV s^{-1}) is the scan rate, and a or b is an empirical constant [2].

$$i(v) = k_1 v\ + k_2 v^{1/2} \#（S5）$$

Or convert it into the following formula:

$$i(v)/v^{1/2} = k_1 v^{1/2} + k_2 \#（S6）$$

Among them, $k_1 v$ and $k_1 v^{1/2}$ represent surface control current and diffusion control

current, respectively [3].

The diffusion coefficient of ions can be calculated using EIS technology, and the formula is as follows:

$$D = \left(R^2T^2\right) / \left(2A^2C^2n^4F^4\sigma^2\right)\#\ (S7)$$

Among them, n is the number of electrons transferred by each molecule in the electronic reaction process, A is the electrode surface area, R is the gas constant, T is the Kelvin temperature, C is the molar concentration of the electrolyte, F is the Faraday constant, and σ is obtained from formula (8);

$$Z' = \sigma\omega^{-0.5} + Rs + Rct\#\ (S8)$$

Among them, Z' is the real part of impedance (Ω), ω is the angular frequency (rad s^{-1}), Rs is the equivalent series resistance (Ω), and Rct is the charge transfer resistance (Ω). The following formulas were used to determine the specific capacity (mAh g^{-1}), energy density (Wh kg^{-1}), and power density (W kg^{-1}):

$$Cm = \frac{2I\int Vdt}{3.6Vm}\#(S9)$$

$$E = \frac{I\int Vdt}{3.6m}\#(S10)$$

$$P = 3600\frac{E}{t}\#(S11)$$

where I (A) represents the discharge current, V (V) denotes the operating voltage, t (s) is the discharge time, and m (g) corresponds to the mass of the active cathode material.

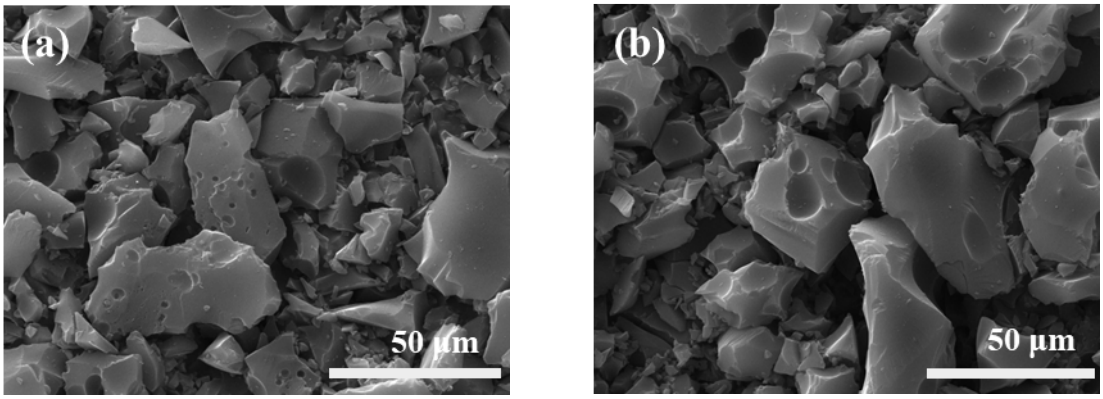

Fig. S1. (a). SEM image of SPC-6-0 after activation, (b). SEM image of SPC-0-20 after activation.

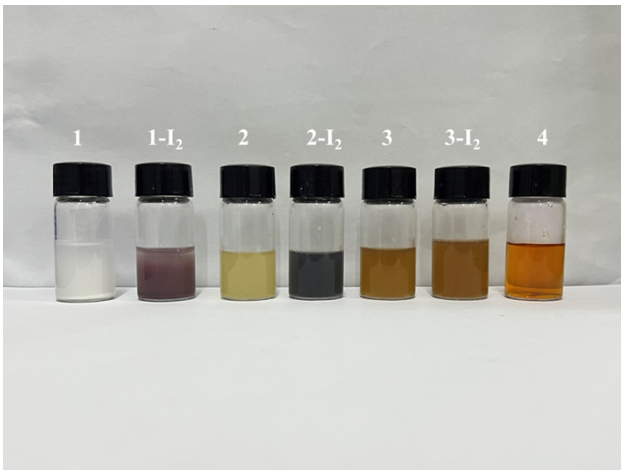

Fig. S2. (1). Starch solution, (2). Add 20ml of starch solution with phosphoric acid, (3). Add 30ml of starch solution with phosphoric acid, (4). iodine solution.

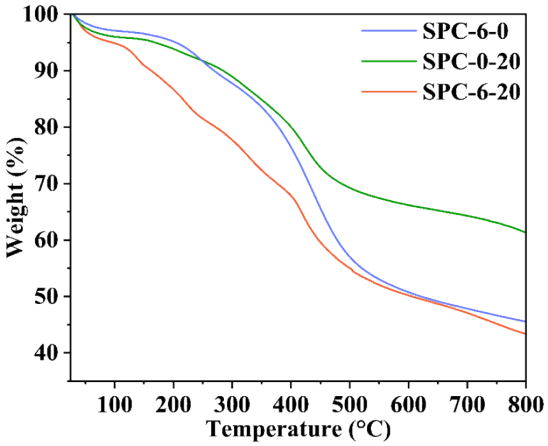

Fig. S3. TG curves for SPC-6-0, SPC-0-20 and SPC-6-20.

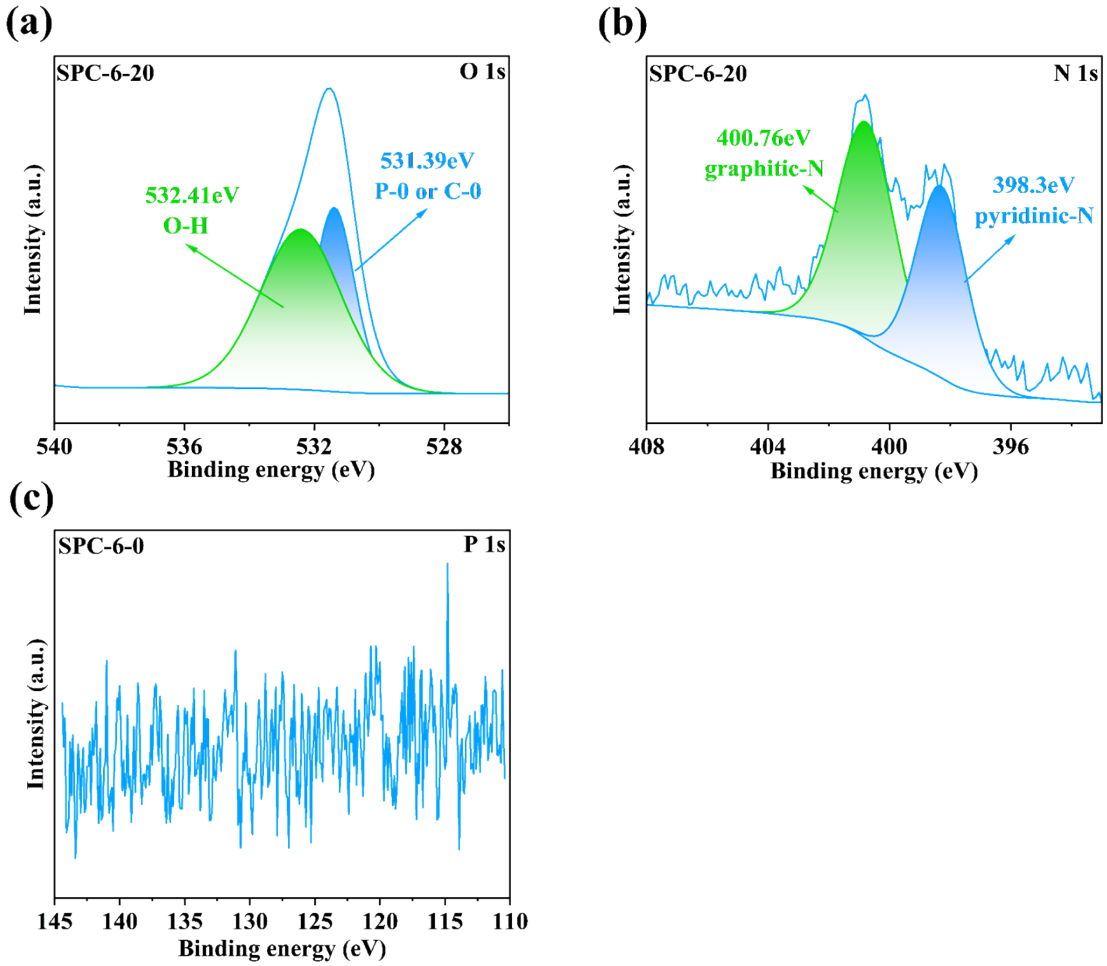

Fig. S4. XPS spectra of SPC-6-20 and SPC-6-0.

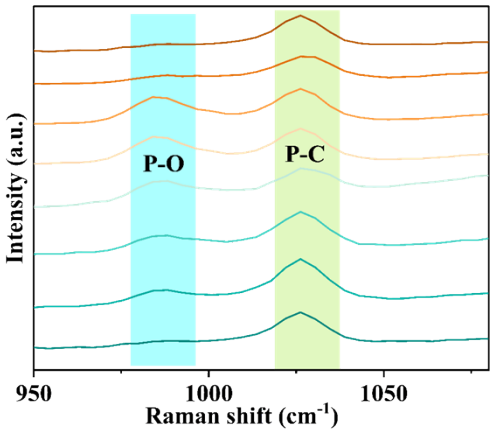

Fig. S5. In situ Raman curve of SPC-6-20.

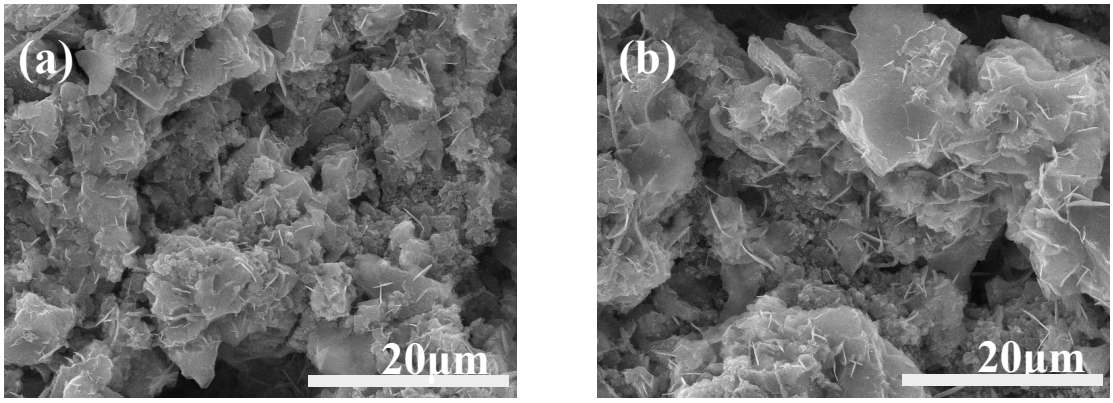

Fig. S6. (a). SEM images of the carbon cathode before SPC-6-20-ZIHC cycling, (b). SEM images of the carbon anode after 60,000 cycles of SPC-6-20-ZIHC at 10 A g^{-1}.

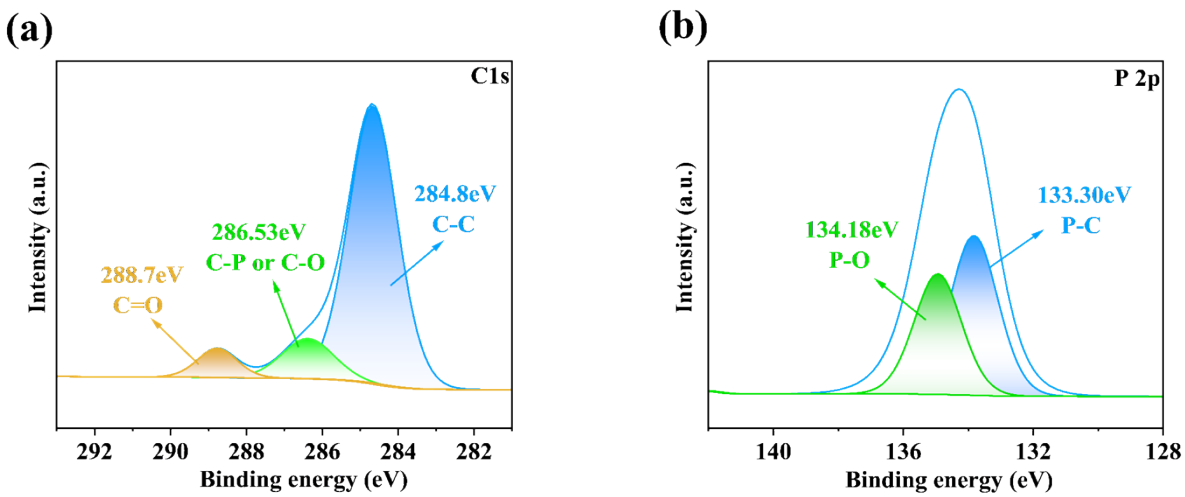

Fig. S7. XPS image of SPC-6-20-ZIHC carbon anode after 60,000 cycles at 10 A g^{-1}.

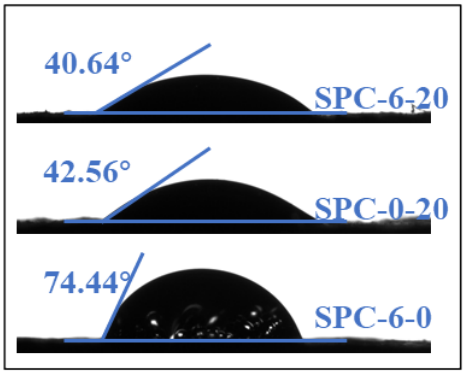

Fig. S8. Water contact angle diagram of SPC-6-0, SPC-0-20 and SPC-6-20.

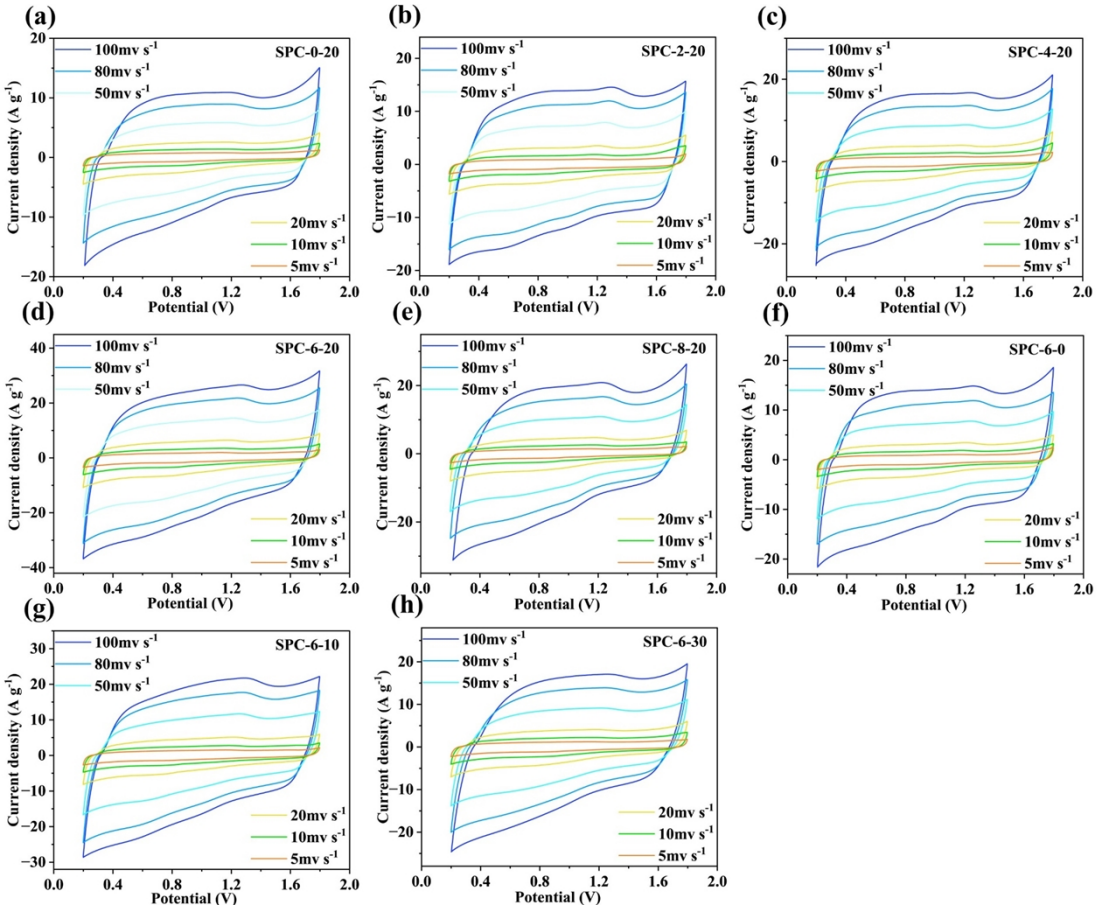

Fig. S9. CV curves of SPC-X-Y tested from 5mV to 100mV.

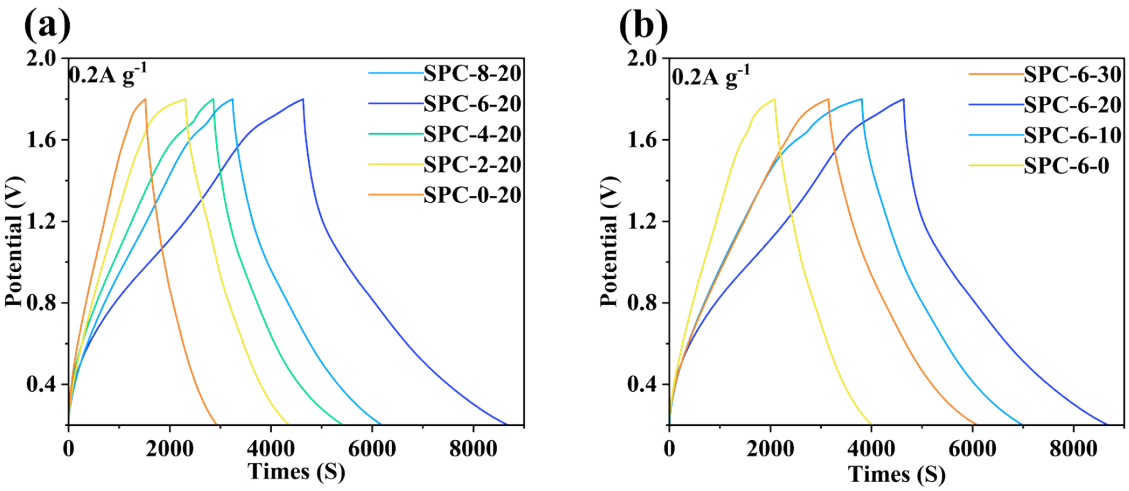

Fig. S10. GCD plot of SPC-X-Y at a current density of 0.2 A g^{-1}.

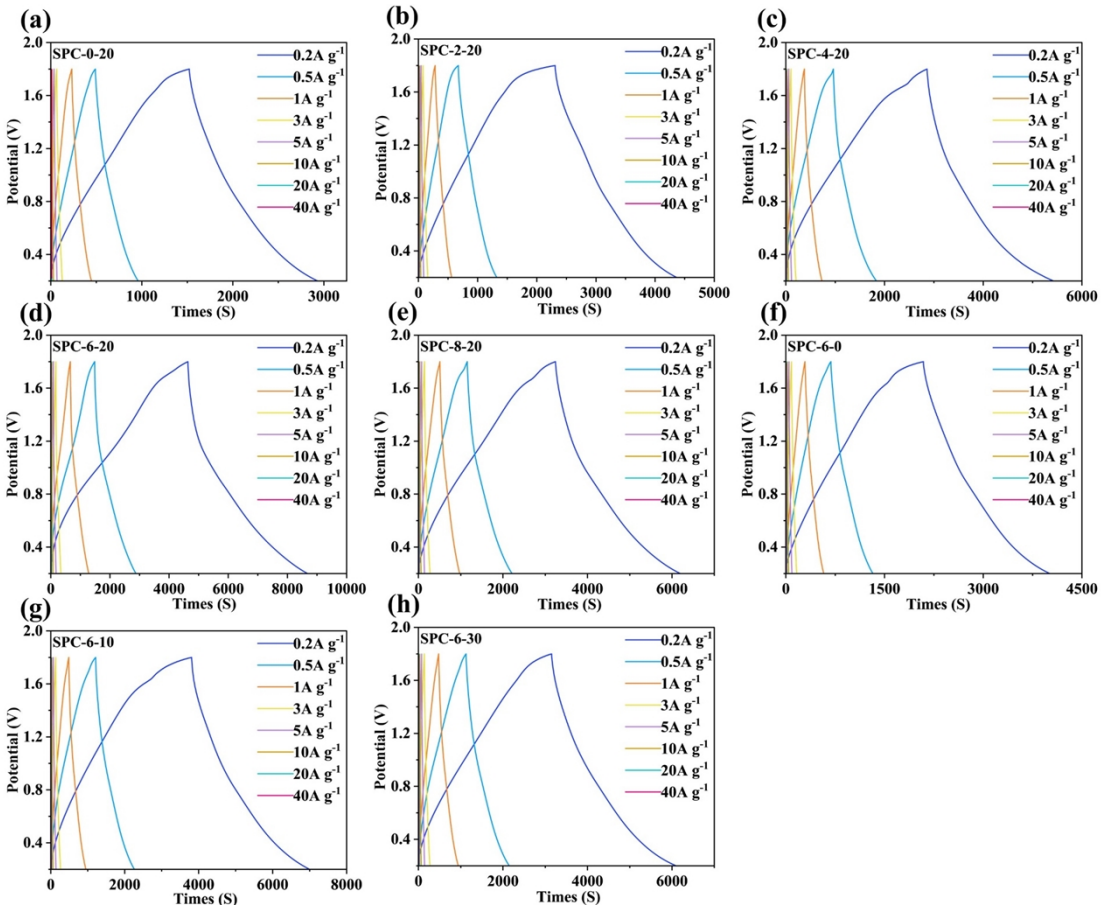

Fig. S11. GCD plot of SPC-X-Y with current density of 0.2 to 40 A g^{-1}.

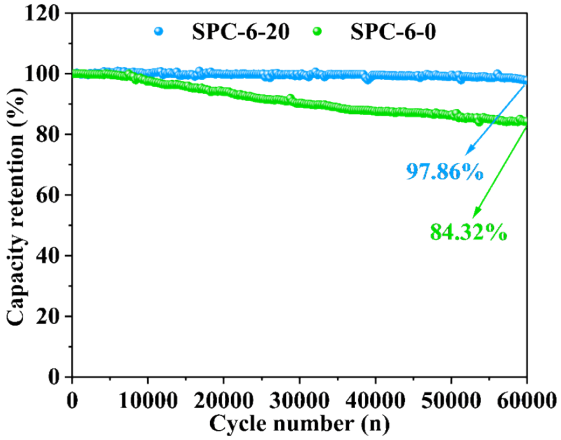

Fig. S12. Cycling stability of SPC-6-20 and SPC-6-0 at 10 A g^{-1}.

Table S1. Comparison of SPC-6-20-ZIHC with previously reported carbon cathodes in terms of activation temperature, specific surface area and pore volume.

Sample	S_{BET} ($m^2\ g^{-1}$)	V_{total} ($cm^3\ g^{-1}$)	Activation temperature (°C)	Ref
OLDC-800	1944.9	0.93	800	4
NPS-HPC	1976.8	1.66	900	5
HC-0.2	1902.9	1.06	800	6
3DPC	2813	1.82	800	7
PPC-800	1163	0.5	800	8
NSLHPC	2705.3	3.27	800	9
HCPC-1-1-800-IMP	1914	0.96	800	10
HPC-800	1941.4	1.34	800	11
C-Zn-Fe	2368	1.13	800	12
$NPFC_{800}$	630.5	0.4	800	13
APHM150	2985.6	1.47	800	14
SPC-6-20	3086.4	2.28	760	This work

Table S2. I_D and I_G Values of SPC-6-20 from In-Situ Raman Testing.

Potential（V）	I_D（cm^{-1}）	I_G（cm^{-1}）	I_D/I_G
0.4	1342.12	1584.47	0.847
0.8	1345.46	1583.64	0.849
1.2	1355.43	1599.42	0.847
1.6	1358.78	1588.43	0.855
1.6	1355.45	1601.34	0.846
1.2	1352.43	1599.42	0.845
0.8	1345.45	1599.42	0.841
0.4	1338.38	1595.42	0.839

Table S3. The corresponding parameters of the EIS spectra of ZHSCs based on SPC-6-20, SPC-0-20 and SPC-6-0.

Sample	Rs (Ω)	Rct (Ω)
SPC-6-20	1.12	6.35
SPC-0-20	1.43	13.15
SPC-6-0	3.32	14.4

Table S4. XPS analysis of SPC-6-20, SPC-6-0 and SPC-0-20.

Sample	XPS analysis (at%)			
	C	O	N	P
SPC-6-20	87.1	8.02	1.67	3.21
SPC-6-0	89.57	9.31	0.83	0.29
SPC-0-20	79.8	17.28	1.55	1.37

Table S5. Elemental analysis of SPC-6-20 and SPC-0-20.

Sample	C (at%)	N (at%)	H (at%)	S (at%)	O (at%)	P (at%)
SPC-6-20	88.87	0.63	0.55	0	7.18	2.77
SPC-6-0	91.14	0.65	0.85	0	7.21	0.15
SPC-0-20	91.83	0.69	1.00	0	3.90	2.58

Table S6. Specific capacity of SPC-X-Y at different current densities.

Sample	Specific capacity (mAh g^{-1})							
	0.2A g^{-1}	0.5 A g^{-1}	1 A g^{-1}	3 A g^{-1}	5 A g^{-1}	10 A g^{-1}	20 A g^{-1}	40 A g^{-1}
SPC-0-20	83.3	69.2	61.1	53.7	50.1	45.9	41.7	37.6
SPC-2-20	109.5	90.2	80.5	70.7	66.2	61.4	56.6	51.1
SPC-4-20	136.1	107.7	96.4	84.1	78.8	71.8	64.4	55.4
SPC-6-20	216.9	176.4	158.5	134.3	125.3	113.1	100.2	91.5
SPC-8-20	166.6	130.3	114.6	99.1	93.5	85.7	79.3	73.2
SPC-6-0	98.8	82.4	73.1	62.6	58.5	52.9	46.5	40.6
SPC-6-10	182.0	135.4	115.3	97.8	93.9	86.8	78.1	67.9
SPC-6-30	147.9	121.1	109.6	93.1	85.8	76.1	65.7	53.7

Table S7. Comparison of energy density and power density between SPC-6-20 based ZIHC and previously reported advanced carbon based ZIHC.

Materials	Electrolyte	Voltage (V)	Energy density (Wh kg^{-1})	Power density (kW kg^{-1})	Ref
GH	2M $ZnSO_4$	0.2-1.8	76.2	6.539	15
L-NS-CNS	1M $ZnSO_4$	0.2-1.8	33.8	9.9	16
Silk-derived AC	PAM/7.5M $ZnCl_2$	0-1.9	217.0	18.0	17
Zn-HSC	1M$Zn(CF_3SO_3)_2$	0-1.8	52.7	1.73	18
NPS-HPC	$Zn(CF_3SO_3)_2$	0.1-1.8	167.69	19.64	5
BCF	2M $ZnSO_4$	0-1.8	58.5	8.7	19
HCS	1M $ZnSO_4$	0.15-1.95	59.7	0.447	20
MnO	1 M Na_2SO_4	0-1.3	55.9	1.24	21
HPC	2M $ZnSO_4$	0-1.8	63.7	3.16	22
PCNs//Zn	2M $ZnSO_4$	0.2-1.8	46	9.77	23
GNPC	1 MLi_2SO_4	0-1.8	46	17.7	24
ACS	6 M KOH	0-1.8	76.6	0.325	25
N-RGO/AAQ-2	2M $ZnSO_4$	0-1.8	50.6	15.6	26
Ca-900	1M $ZnSO_4$	0-1.8	43	0.88	27
CNPK	1M $ZnSO_4$	0.2-1.8	8.5	4.25	28

Table S8. Comparison of electrochemical properties of SPC-6-20-based ZIHC with previously reported advanced carbon-based ZIHCs.

Materials	Electrolyte	Voltage (V)	Energy density (Wh kg^{-1})	Power density (kW kg^{-1})	Cycling stability	Ref
3D HPC	2M $ZnSO_4$	0.01-1.8	118	3.158	94.9% (20000 cycles) 2A g^{-1}	22
HCS	1M $ZnSO_4$	0.15-1.95	59.7	0.447	98% (15000 cycles) 1A g^{-1}	20
Silk-derived AC	PAM/7.5M $ZnCl_2$	0-1.9	217.0	18.0	95.1% (100000 cycles) 5A g^{-1}	17
NPS-HPC	$Zn(CF_3SO_3)_2$	0.1-1.8	167.69	19.64	99.98 %(23000 cycles)5A g^{-1}	5
GH	2M $ZnSO_4$	0.2-1.8	76.2	6.539	90% (10000 cycles) 15A g^{-1}	15
GNPC	1 MLi_2SO_4	0-1.8	46	17.7	95%(10000 cycles)5A g^{-1}	24
MXene-rGO	2M$ZnSO_4$	0.2-1.6	34.9	4.0	95% (75000 cycles) 5A g^{-1}	29
Zn-MET-800	2M $ZnSO_4$	0.1-1.7	128.5	4.7	90.3%(30000 cycles)10A g^{-1}	30
PC800	3M $Zn(ClO_4)_2$	0-1.9	108.4	48.8	99.2% (30000 cycles) 20A g^{-1}	31
NTC	1M $ZnSO_4$	0-2	189.6	11.26	80.5% (10000 cycles) 5A g^{-1}	32
CB-3-850	6M KOH	0-1.8	73.8	14.8	90% (10000 cycles) 20A g^{-1}	33
PN-CHoNS	2 M $ZnSO_4$	0.2-1.8	116	21.66	80.6% (12000 cycles) 5A g^{-1}	34
P/B-AC	2 M $ZnSO_4$	0.2-1.8	169.4	20	88% (30000 cycles) 10A g^{-1}	35
WAPC-4/P	2 M $ZnSO_4$	0.3-1.9	127.1	1.6	88.2%（15000 cycles7.5A g^{-1}	36
HPC/CC	2 M $ZnSO_4$	0.2-1.8	110	20	95.7% (10000 cycles) 5A g^{-1}	37
SPC-6-20	2 M $ZnSO_4$	0.2-1.8	168.79	31.52	97.86% (60000 cycles) 10A g^{-1}	This work

References

1. J. Xiong, X. Li, J. Huang, X. Gao, Z. Chen, J. Liu, H. Li, B. Kang, W. Yao and Y. Zhu, *Applied Catalysis B: Environmental*, 2020, **266**, 118602.
2. Y. Long, X. An, H. Zhang, J. Yang, L. Liu, Z. Tian, G. Yang, Z. Cheng, H. Cao, H. Liu and Y. Ni, *Chemical Engineering Journal*, 2023, **451**, 138877.
3. Z. Li, D. Chen, Y. An, C. Chen, L. Wu, Z. Chen, Y. Sun and X. Zhang, *Energy Storage Materials*, 2020, **28**, 307-314.
4. H. Li, P. Su, Q. Liao, Y. Liu, Y. Li, X. Niu, X. Liu and K. Wang, *Small*, 2023, **19**, 2304172.
5. S. Wang, F. Wei, W. Geng, Z. Ren and Y. Lv, *Chemical Engineering Journal*, 2025, **515**, 163462.
6. H.-X. Li, W.-J. Shi, L.-Y. Liu, X. Zhang, P.-F. Zhang, Q. Wang, Y. Liu, Z.-Y. Wang and J. Dou, *Chemical Engineering Journal*, 2024, **487**, 150630.
7. Y. Wang, J. Yang, S. Liu, X. Che, S. He, Z. Liu, M. Wang, X. Wang and J. Qiu, *Carbon*, 2023, **201**, 624-632.
8. D. Zhang, W. Ma, J. Wang, X. Lu and J. Luo, *Journal of Energy Storage*, 2025, **117**, 116236.
9. Y. Fan, F. Fu, D. Yang, W. Liu and X. Qiu, *Journal of Colloid and Interface Science*, 2024, DOI: 10.1016/j.jcis.2024.04.099.
10. P. Zhang, Y. Chen, X. Song, H. Zhang, J. Cui and B. Wang, *Chemical Engineering Journal*, 2024, DOI: 10.1016/j.cej.2024.157703.
11. Y. Wang, R. Liu, Y. Tian, Z. Sun, Z. Huang, X. Wu and B. Li, *Chemical*

Engineering Journal, 2019, DOI: 10.1016/j.cej.2019.123263.

12. Q. Liu, T. Wang, D. Jia, P. Ren and D. Wu, *Advanced Functional Materials*, 2025, **35**, 2500016.
13. F. Wei, Y. Wei, J. Wang, M. Han and Y. Lv, *Chemical Engineering Journal*, 2022, **450**, 137919.
14. Y. Lu, G. Zhou, Z. Zhang, C. Li, Q. Dong, Y. Su and W. Chen, *Chemical Engineering Journal*, 2025, DOI: 10.1016/j.cej.2025.161085.
15. Y. Zhu, X. Ye, H. Jiang, J. Xia, Z. Yue, L. Wang, Z. Wan, C. Jia and X. Yao, *Journal of Power Sources*, 2020, **453**, 227851.
16. W. Jian, W. Zhang, X. Wei, B. Wu, W. Liang, Y. Wu, J. Yin, K. Lu, Y. Chen, H. N. Alshareef and X. Qiu, *Advanced Functional Materials*, 2022, **32**, 2209914.
17. C. Wang, Z. Pei, Q. Meng, C. Zhang, X. Sui, Z. Yuan, S. Wang and Y. Chen, *Angewandte Chemie International Edition*, 2021, **60**, 990-997.
18. H. Wang, M. Wang and Y. Tang, *Energy Storage Materials*, 2018, **13**, 1-7.
19. H. Fan, X. Hu, S. Zhang, Z. Xu, G. Gao, Y. Zheng, G. Hu, Q. Chen, T. S. AlGarni and R. Luque, *Carbon*, 2021, **180**, 254-264.
20. S. Chen, L. Ma, K. Zhang, M. Kamruzzaman, C. Zhi and J. A. J. J. o. M. C. A. Zapien, *Journal of Materials Chemistry A*, 2019, **7**, 7784-7790.
21. S. Dang, Y. Wen, T. Qin, J. Hao, H. Li, J. Huang, D. Yan, G. Cao and S. Peng, *Chemical Engineering Journal*, 2020, **396**, 125342.
22. P. Yu, Y. Zeng, Y. Zeng, H. Dong, H. Hu, Y. Liu, M. Zheng, Y. Xiao, X. Lu and Y. Liang, *Electrochimica Acta*, 2019, **327**, 134999.

23. J. Zhang, F. Qin, P. Zuo and W. Shen, *ChemSusChem*, 2025, **18**, e202401311.

24. J. Li, Y. Gao, R. Holze, S. Li, E. Mijowska and X. Chen, *Batteries & Supercaps*, 2023, **6**, e202300175.

25. C. Li, J. Balamurugan, D. C. Nguyen, N. H. Kim and J. H. Lee, *ACS Applied Materials & Interfaces*, 2020, **12**, 21505-21514.

26. W. Zhang, H. Kang, Z. Gu, H. Liu, Z. Li, X. Li and B. Yang, *Journal of Energy Storage*, 2023, **61**, 106715.

27. Y. Zhang, Z. Wang, D. Li, Q. Sun, K. Lai, K. Li, Q. Yuan, X. Liu and L. J. J. o. M. C. A. Ci, *Journal of Materials Chemistry A*, 2020, **8**, 22874-22885.

28. H. Zhang, Z. Chen, Y. Zhang, Z. Ma, Y. Zhang, L. Bai and L. J. J. o. M. C. A. Sun, *Journal of Materials Chemistry A*, 2021, **9**, 16565-16574.

29. Q. Wang, S. Wang, X. Guo, L. Ruan, N. Wei, Y. Ma, J. Li, M. Wang, W. Li and W. Zeng, *Advanced Electronic Materials*, 2019, **5**, 1900537.

30. D. Jia, Z. Shen, W. Zhou, Y. Li, J. He, L. Jiang, Y. Wei and X. He, *Chemical Engineering Journal*, 2024, **485**, 149820.

31. J. Yin, W. Zhang, W. Wang, N. A. Alhebshi, N. Salah and H. N. Alshareef, *Advanced Energy Materials*, 2020, **10**, 2001705.

32. R. Yuksel, O. Buyukcakir, P. K. Panda, S. H. Lee, Y. Jiang, D. Singh, S. Hansen, R. Adelung, Y. K. Mishra, R. Ahuja and R. S. Ruoff, *Advanced Functional Materials*, 2020, **30**, 1909725.

33. P. Liu, F. Kong, H. Tang, Y. Wu, X. Xu, J. Zhao, X. Liu, Z. Deng, J. Li, S. Chen, J. Zou and J. Peng, *Chemical Engineering Journal*, 2024, **491**, 151944.

34. J. Li, J. Zhang, L. Yu, J. Gao, X. He, H. Liu, Y. Guo and G. Zhang, *Energy Storage Materials*, 2021, **42**, 705-714.

35. Y.-G. Lee and G.-H. An, *ACS Applied Materials & Interfaces*, 2020, **12**, 41342-41349.

36. S. Haibin, L. Congcong, G. Dongfang, L. Shuangshuang, X. Wenhe, L. Shenghong and L. Zijiong, *RSC advances*, 2022, **12**, 24724-24733.

37. X. Deng, J. Li, Z. Shan, J. Sha, L. Ma and N. J. J. o. M. C. Zhao, *Journal of Materials Chemistry A*, 2020, **8**, 11617-11625.